Synthesis of Si Nanosheets by a Chemical Vapor Deposition Process and Their Blue Emissions

Ungkil Kim,[†] Ilsoo Kim,[†] Yonghee Park,[†] Ki-Young Lee,[†] Sang-Youp Yim,[‡] Jae-Gwan Park,[§] Hong-Gyu Ahn,[⊥] Seung-Han Park,[⊥] and Heon-Jin Choi[†,*]

[†]School of Advanced Materials Science and Engineering, Yonsei University, Seoul 120-749, South Korea, [‡]Advanced Photonics Research Institute (APRI), Gwangju Institute of Science and Technology (GIST), Gwangju 500-712, South Korea, [§]Nano-Science Research Division, Korea Institute of Science and Technology (KIST), Seoul 136-791, South Korea, and [⊥]Department of Physics, Yonsei University, Seoul 120-749, South Korea

ABSTRACT We synthesized free-standing Si nanosheets (NSs) with a thickness of about <2 nm using a chemical vapor deposition process and studied their optical properties. The Si NSs were formed by the formation of frameworks first along six different ⟨110⟩ directions normal to [111], its zone axis, and then by filling the spaces between the frameworks along the ⟨112⟩ directions under high flow rate of processing gas. The Si NSs showed blue emission at 435 nm, and absorbance and photoluminescence (PL) excitation measurements indicate that enhanced direct band transition attributes to the emission. Time-resolved PL measurement, which showed PL emission at 435 nm and a radiative lifetime of 1.346 ns, also indicates the enhanced direct band gap transition in these Si NSs. These outcomes indicate that dimensionality of Si nanostructures may affect the band gap transition and, in turn, the optical properties.

KEYWORDS: silicon · nanosheets · photoluminescence · ultrathin two-dimensional formation · enhanced direct band gap transition

Zero-dimensional (0D) and one-dimensional (1D) silicon (Si) nanostructures, such as Si quantum dots or nanowires, have unique chemical and physical properties of high surface area and size-confinement effects.[1−4] It is also known that the two-dimensional (2D) nanostructures have different properties than 0D or 1D nanostructures. For example, 2D carbon nanostructures, such as graphene, have unique properties over the 0D or 1D nanostructures, such as fullerene and carbon nanotubes, respectively, and, thus, have been considered as a building block for many novel applications.[5−7] In this regard, 2D Si nanostructures should be interesting for exploring their potential in many applications.

While the synthesis and properties of 0D and 1D Si nanostructures (quantum dots and nanowires, respectively) have been widely reported in previous studies, 2D Si nanostructures are rarely reported.[8−11] In the limited studies, Si nanosheets (NSs) as 2D Si nanostructures have been synthesized by using solution-based methods.[9−11] However, they are not a free-standing structure but a hybrid structure composed of Si−Ca or Si−methylamines.[10,11] Therefore, it is uncertain whether they retain intrinsic Si characteristics, such as the ability to operate as a semiconductor. Synthesis of free-standing, 2D Si nanostructures is thus crucial to address the properties of 2D Si nanostructures. Akin to Si quantum dots or nanowires, synthesis of 2D Si nanostructures by a complementary metal-oxide-semiconductor (CMOS)-compatible process as well as solution-based process should also be interesting by considering their potential in many electronic devices that are typically fabricated by the CMOS process.

Herein, we report the synthesis of free-standing, 2D Si NSs by a chemical vapor deposition (CVD) process along with their optical properties. These single-crystalline Si NSs, which are very thin with a thickness of <2 nm, were grown under a high flow rate of processing gas. They show unique optical properties of blue emission with a wavelength of 435 nm and a radiative lifetime of 1.346 ns that would be ascribed to the enhanced direct band gap transition.

RESULTS AND DISCUSSION

Figure 1a−c shows typical scanning electron microscopy (SEM) images of Si NSs grown on a Si substrate. As shown in Figure 1a, sphere-shaped materials were formed on the substrate. They look like a wad of cotton wool with a diameter of about 30 μm. However, upon closer observation, a great number of small NSs were observed (Figure 1b,c). It was difficult to

* Address correspondence to hjc@yonsei.ac.kr.

Received for review December 9, 2010 and accepted January 28, 2011.

Published online February 15, 2011
10.1021/nn103385p

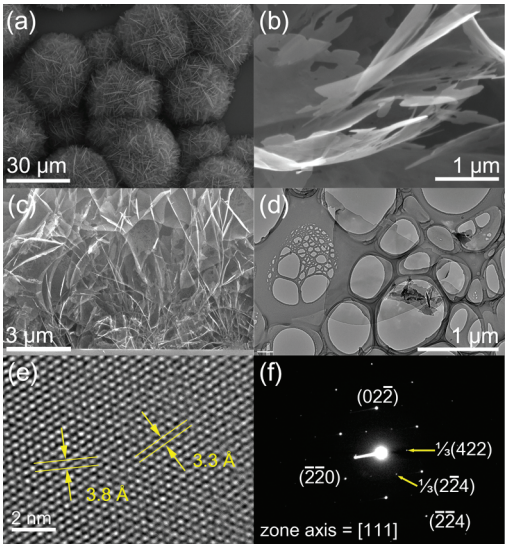

Figure 1. (a,b) Typical SEM images of Si NSs grown on a Si substrate with a growth time of 30 min. (c) SEM image of cross-sectioned substrate. (d) Typical low-magnitude TEM image of Si NSs. (e) HRTEM image of Si NSs, showing the single-crystalline nature of the Si NS. (f) SAED pattern of Si NSs, indicating that its stacking axis is in the [111] direction, and showing the $^1/_3$(422) forbidden spots.

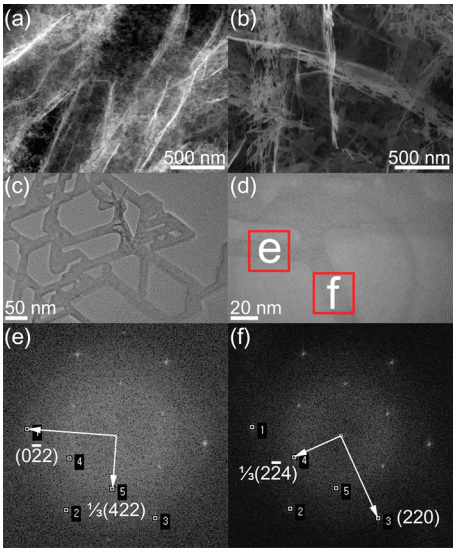

Figure 2. (a,b) Typical SEM images of Si NSs grown on a Si substrate with a growth time of 5 and 10 min, respectively. (c–f) Low- and high-magnitude TEM images of frameworks in the initial stage during the formation of Si NSs (c,d) and its FFT patterns (e,f), indicating that the growth direction of the frameworks is six different ⟨110⟩ directions normal to [111] and that filling process occurs along the ⟨112⟩ directions.

determine the thickness of individual Si NSs as they were too thin to be characterized precisely using AFM or other characterization tools. We roughly estimated the thickness of the NSs as a few nanometers; however, it was likely closer to 2 nm according to the contrast in the high-resolution transmission electron microscopy (HRTEM) images taken of very thin Si nanowires with a diameter of 4 nm (Figure S1, Supporting Information). A number of holes were observed inside the NSs, which are relevant to the growth mechanism, as will be discussed later.

Figure 1d shows a typical transmission electron microscopy (TEM) image of Si NSs. The thickness of the NSs is very thin, allowing it to be transparent under TEM observation. Figure 1e shows a HRTEM image of an individual Si NS, showing its single-crystalline nature. Each lattice spacing of the (112) and (110) planes matches those of the Si. A selected area electron diffraction (SAED) pattern recorded from the NS, as shown in Figure 1f, indicates that the stacking axis is in the [111] direction, also showing the $^1/_3$(422) forbidden spots that arise due to the lack of an ABC stacking plane in thin films or nanowires.[12,13] An energy-dispersive spectroscopy (EDS) analysis showed that the NSs are pure Si without any other impurities or elements. The Si NSs were also characterized using X-ray diffraction (XRD), showing that all of the peaks were indexed to a Si diamond structure (Figure S2, Supporting Information).

The growth mechanism is interesting because the growth of such a very thin, free-standing 2D Si nanostructure by a CVD process has not been observed thus far. To address the formation of the Si NSs, we observed their growth over time. Figure 2a,b shows typical SEM images of Si NSs grown for 5 and 10 min, respectively. A large number of tiny threads became entangled with a faint formation of sheets at an early stage (Figure 2a), which then evolved into more fully formed sheets (Figure 2b). Bridge-like structures were also observed in each sheet, as shown in Figure 2b. This observation suggests that the Si NSs were formed by the growth of frameworks first and then fill out the void between the frameworks. It is worth noting that the holes inside the NSs have a triangle or hexagon shape (Figure S3, Supporting Information). This indicates that the frameworks grew in six different directions at the initial stage.

These frameworks were further investigated using HRTEM together with the fast Fourier transform (FFT) pattern. Figure 2c,d shows low- and high-magnitude TEM images of a Si NS sample grown for 10 min, showing that the frameworks formed into a hexagonal structure before they were filled completely. Figure 2e, f shows the FFT patterns of the regions indicated by the red square box in Figure 2d. Regardless of the position, the FFT results show the same pattern in all frameworks constituting a single network. Both of them also showed the [111] zone axis. These results indicate that the frameworks in the same sheet were formed by single-crystal growth and that they grew in six directions of ⟨110⟩ normal to [111], its stacking axis, with a side face of {112}. Therefore, on the basis of observations through SEM and TEM, it can be suggested that the Si NSs were formed by the formation of frameworks first along six different ⟨110⟩ directions normal to [111], its zone axis, and then by filling the spaces between the frameworks along the side face, ⟨112⟩ directions.

The preferred growth along the ⟨110⟩ and ⟨112⟩ directions at the initial stage can be attributed to the minimization of the total surface energy by exposure of the (111) planes.[13−15] In fact, previous reports have also shown that 1D growth of Si along the ⟨110⟩ direction is thermodynamically more favorable when the diameter is very small, less than 10 nm.[13]

The TEM characterization indicates that the frameworks grown in ⟨110⟩ directions have an epitaxial relation with each other and thus are in the same plane because there are 12 [110] directions in regard of one [111] direction and six of them are in-plane with the [111] direction. It is noted that the frameworks can also grow in the other six out-of-plane [110] directions in the course of growth. As a result, Si NSs grow randomly in a macroscopic spatial dimension and become a spherical shape, as shown in Figure 1a.

It is interesting that the growth along the stacking axis, [111], is suppressed in the course of growth along the ⟨110⟩ direction, thus resulting in the growth of 2D NSs. According to our systematic investigation, the critical factor for the formation of NSs is a high flux of hydrogen (H_2) gas. In fact, a low flux of H_2 only resulted in the growth of nanowires, and a high flux of helium or argon (Ar) resulted in the deposition of thin films. Therefore, it can be explained in terms of the kinetic as well as the chemical effect of a high flow rate of H_2 on the growth of Si nanostructures. Because H_2 and Si chloride ($SiCl_4$) were used in our process, H_2 passivation and chlorination were expected on the surface of the Si crystals along the growth process. It is known that the effect of these chemical functionalization processes on the surface states depend on the orientation of the surfaces; that is, the ⟨100⟩ surfaces of Si become very rough, while the ⟨111⟩ surfaces maintain smoothness on an atomic scale in the course of H_2 passivation and chlorination.[16,17] It is also known that the incorporation of Si atoms on the smooth plane for the crystal growth is rather difficult, leading to slower growth or even stop as compared to a rough surface (*e.g.*, ⟨100⟩ or ⟨110⟩).[18] In addition, the high flow rate of the H_2 gas in our process can enforce these chemical functionalization processes *via* a dynamic kinetic effect; that is, it enhances the chemical reactions by increasing the effective collisions or impingement of atoms from the vapor to the surface of the Si. Therefore, by the enforced chemical functionalization, the growth rate in ⟨111⟩ and ⟨110⟩ directions can become significantly different and result in the 2D growth of Si nanostructures. It is noted that the 1D framework growth in the ⟨110⟩ direction occurs without the aid of catalyst, while typical 1D Si nanostructure (*e.g.*, Si nanowires) growth occurs with the aid of catalyst. As described, it may be due to the chemical functionalization that induces significant different growth rate between ⟨111⟩ and ⟨110⟩ directions. The morphology of Si NSs supports the idea of the critical role of different growth rate on the formation of Si NSs. As shown in Figure 1b and Figure S3, Si NSs have void frameworks at the edges. It would be due to the formation of the NSs by the growth of frameworks first and then fill out the void between the frameworks. When the growth rates between ⟨110⟩ and ⟨112⟩ directions are different, the frameworks continuously grow and branch off in the fill-out stage, and each Si NS has a void framework at the edges.

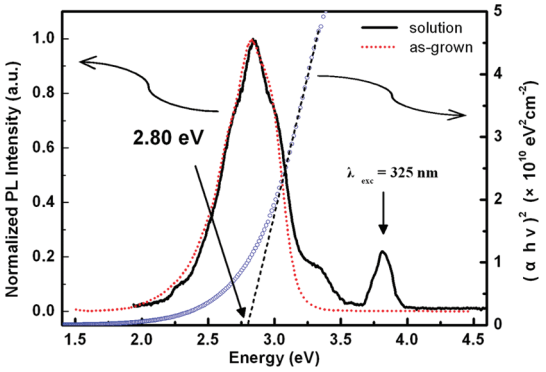

Figure 3. Room-temperature PL spectra of Si NSs dispersed in an ethanol solution (black, solid) and as-grown Si NSs (red, dotted) excited by a wavelength of 325 nm (indicated by a vertical arrow) using a He−Cd laser. Two PL emissions at 435 nm are similar to the optical band gap for the direct transition (E_d) of ∼2.80 eV (blue circle) as calculated from the absorbance measurements.

The optical properties of Si NSs were investigated by photoluminescence (PL) and absorbance measurements. Figure 3 shows the normalized PL spectrum of Si NSs dispersed in an ethanol solution (black, solid). The vertical arrow in the right part of Figure 3 indicates the wavelength (325 nm) of the excitation source. The PL spectrum of as-grown Si NSs grown on a Si substrate (red, dotted) is also shown in Figure 3 for comparison. The PL spectrum of the NSs (black, solid) exhibited a broad peak with maximum intensity around 435 nm (2.85 eV), which is similar to that of the as-grown NSs (red, dotted). Other Si NSs grown on sapphire, gallium nitride (GaN), or quartz substrates also showed similar PL results. The emission at 435 nm matches the optical band gap well for a direct transition (E_d) of ∼2.80 eV (blue circle), as calculated from the absorbance measurement (Figure S4b, Supporting Information). Furthermore, this main emission energy of the NSs is identical to those of previous reports on 2D Si NSs.[10,11]

To investigate the origin of the PL from the NSs, we performed the absorbance measurement of Si NSs. The spectrum in Figure S4a shows its peaks at 306 and 364 nm with an indirect absorption tail. The peak at 306 nm is associated with a direct transition at the Γ point [$\Gamma_{25} \rightarrow \Gamma_{2'}$] or possibly a direct transition at X in the bulk Si, whose energy is 4.2 eV (295 nm), while the second peak at 364 nm is associated with a direct transition at the Γ point [$\Gamma_{25} \rightarrow \Gamma_{15}$] comparable to 3.4 eV (365 nm) in the bulk Si.[19] This absorption result did not show a

blue shift at the absorption edges, as observed in previous studies of 0D Si quantum dots, 1D Si nanowires, and 2D hybrid Si NSs.[10,11,20−24] Instead, a greatly enhanced direct transition as compared to an indirect transition was observed in this study. As shown in Figure S4a, the values of the absorption peaks are identical to those of bulk Si; however, the absorption spectrum of the NSs increases sharply only in the region of a short (high) wavelength (energy). This indicates that the direct transitions are improved while the indirect transition is suppressed as compared to the case of bulk Si.

We also calculated the absorption coefficient, α, and the optical band gap, E_g, for Si NSs based on the measured absorbance (Figure S4, Supporting Information). The result showed that linear extrapolation to zero yields an optical band gap of the NSs for a direct transition (E_d) and for an indirect transition (E_i), 2.8 and 1.73 eV, respectively. It was noted that these band gaps are larger than that of bulk crystalline Si (~1.1 eV) and even amorphous Si (~1.5 eV), which may exist on the surface of the NSs.[25] Therefore, the attribution of a very thin amorphous Si shell to the observed values of E_d and E_i can be safely excluded. The possible attribution of a native oxide layer to the observed PL emission can also be excluded because PL excitation and emission measurements, as follows, showed that the oxidized surface is not relevant to the PL emission at 435 nm.

To clarify whether the PL comes from the Si NSs, we further performed PL excitation and emission measurements of the Si NSs. Figure 4a shows the PL emission (black, solid) and excitation (red, dotted) spectra along with the absorbance spectrum (blue circle). The vertical solid and dotted arrows indicate the wavelengths of the excitation source (360 nm) and detection energy (435 nm), respectively. The emission was observable by the naked eye (inset in the upper right part of Figure 4a) when exposed to UV light with a wavelength of 365 nm. The spectra in Figure 4a exhibit an excitation peak at 367 nm (red, dotted) and a PL emission maximum of 437 nm (black, solid). These results indicate that the PL emission of the Si NSs at 437 nm is caused by the absorption at 367 nm, which is consistent with the absorption peak at 365 nm (blue circle). It further indicates that the origin of the PL is the Si NSs. As the absorption at this peak is associated with the direct transition at the Γ point [$\Gamma_{25} \rightarrow \Gamma_{15}$] of the bulk Si,[19] and considering the absorbance data (Figure S4a), which show the characteristic of bulk Si (no blue shift) but an enhanced direct transition, it is highly likely that the PL of Si NSs stems from the enhanced direct band transition.

There have been many theoretical and experimental studies on 0D and 1D Si nanostructures showing PL in the visible region,[19,23,26−28] while there are only limited studies on the 2D Si nanostructures.[8−11] In these studies, the visible emission from 2D Si nanostructures

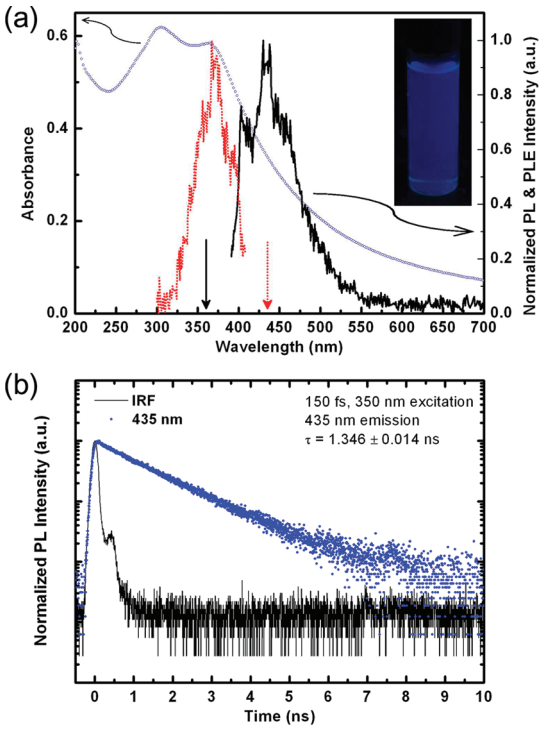

Figure 4. (a) Spectra of PL emission (black, solid) and excitation (red, dotted) measured using a UV lamp. The solid and dotted arrows indicate the excitation (360 nm) and detection energy (435 nm), respectively. The inset shows an image exhibiting the luminescent emission from an ethanol solution containing Si NSs when exposed to UV light. The absorbance spectrum (blue circle) also appears in the figure. (b) Time-resolved PL spectrum of Si NSs (blue dotted) dispersed in an ethanol solution using an excitation wavelength of 350 nm. The decay was recorded at an emission wavelength of 435 nm.

has explained by direct electron−hole recombination as 0D Si nanostructures (*e.g.*, Si quantum dots). However, our characterizations indicate that the direct band gap transition is responsible for the luminescence. One possible explanation on this enhanced direct band gap transition is the compressive strain in the Si NSs. It was reported that 2D nanostructures are under compressive strain due to surface tension,[29] and that the compressive strain can induce an indirect−direct band gap transition in Si or other nanostructures.[30,31] Therefore, the compressive strain in Si NSs could enhance the direct band gap transition and induce the blue emission.

The result of time-resolved PL (TR-PL) measurement further supports the fact that the PL from Si NSs is associated with the direct band gap transition at 365 nm. Figure 4b shows the TR-PL spectrum of Si NSs (blue dotted) dispersed in an ethanol solution. On the basis of the PL spectrum (Figure S5, Supporting Information), the decay was recorded at an emission wavelength of 435 nm. The radiative lifetime (τ = 1.346 ns) was obtained from the TR-PL measurement. It was found to be comparable to that of direct-like $e-h$ recombination, as in bulk GaAs, while significantly different from

that of bulk Si, τ being on the order of tens of microseconds to milliseconds. It is notable as well that the radiative lifetime has only a single component, unlike silica nanotubes and nanodisks, which have two components.[32] Rather, this finding is similar to a previous reported case of a Si nanocrystal sample with a diameter of 3 nm,[19] except that we were not able to observe the fast initial component of huge amplitude with τ being on the order of tens of picoseconds because it was within our measurement errors.

In summary, the present study reports a free-standing, single-crystalline Si NS grown using a CVD process along with its structural and optical properties. SEM and HRTEM observations with FFT patterns indicate that these Si NSs were formed by the formation of frameworks first along six different ⟨110⟩ directions normal to [111], its zone axis, and then by filling the spaces between the frameworks along the ⟨112⟩ directions. A high flow rate of H_2 was revealed as a critical factor in the growth of the Si NSs. The PL and absorption characteristics showed that the direct transitions in the NSs were improved compared to those of the bulk Si and that the PL of the NSs is associated with the enhanced direct transition. These results are further supported by the result of time-resolved PL measurement, which showed PL emission at 435 nm and a radiative lifetime of 1.346 ns. These outcomes indicate that dimensionality significantly affects the band gap transition and, in turn, the optical properties of Si nanostructures. It also indicates that the Si NSs in this study are optically active and thus can be used to develop Si optoelectronics.

EXPERIMENTAL SECTION

Synthesis of Si NSs. Si NSs were successfully synthesized on various substrates, including Si, sapphire, GaN, and quartz, using a CVD process in a high-flux H_2 environment. No catalyst was used for the growth. Prior to grow Si NSs, conventional wet chemical cleaning processes were performed to remove any contaminations on the substrates. The substrates were then placed at a center of a hot-wall horizontal reactor by using quartz tray. The temperature of the reactor was increased at a rate of 35 °C min^{-1} to the reaction temperature of 1000 °C under a H_2 (99.9999%) and an Ar (99.9999%) atmosphere, a flow rate of 3000 and 100 sccm, respectively. Silicon chloride ($SiCl_4$, Aldrich, 99.999%) was then introduced into the reactor by bubbling with H_2 carrier at a flow rate of 20 sccm. The liquid $SiCl_4$ was held at 0 °C using a chiller. After 30 min, it was turned off, and then the reactor was cooled to room temperature under the same H_2 and Ar atmosphere.

Structural Characterization. The structural properties of the Si NSs were characterized using SEM (Hitachi 3000) and TEM (JEOL 7100, 200 keV). To prepare the samples for TEM observation, the NSs were first dispersed and sonicated in an ethanol solution. A small droplet of the solution was then dropped onto the copper TEM grid. The XRD measurements were performed using high-resolution X-ray diffractometry at the 11A beamline of the Pohang Accelerator Laboratory. An X-ray of source energy of 10 keV was used.

Optical Characterization. For all measurements, Si NSs were dispersed in ethanol and the solutions were put into a quartz cuvette (Hellma, 111-QS) with a path length of 1 cm. All of the measured data were corrected for the ethanol cuvette background. The PL measurement of Si NSs grown on a Si substrate was performed using a He−Cd laser of 3 mW with an excitation wavelength of 325 nm. The absorbance of the Si NSs was measured using a UV−visible spectrophotometer (JASCO, V-570) (Figure S4a, Supporting Information). The absorption coefficient α and the optical band gap E_g for the Si NSs based on the measured absorbance were determined using the following equation:[33]

$$\alpha = \frac{2.303 \times 10^3 \times A\rho}{lC} \quad (1)$$

$$\alpha h\nu \propto (h\nu - E_g)^n \quad (2)$$

Here, A is the absorbance of a sample; ρ is the density of Si, 2.33 g cm^{-3}; C is the concentration of the particles in g·L^{-1}; l is the path length of the sample; and n is $^1/_2$ for a direct transition and 2 for an indirect transition. The optical band gap of the Si NSs for a direct transition and for an indirect transition, E_d and E_i, was determined by plotting $(\alpha h\nu)^2$ and $(\alpha h\nu)^{1/2}$, respectively, *versus* the photon energy (Figure S4b,c, Supporting Information). PL emission and excitation spectra of the Si NSs were recorded by a spectrofluorometer (Jobin Yvon Inc., Fluorolog 3) equipped with a 450 W Xe lamp with a spectral resolution of 1 nm. Time-correlated single-photon counting (TCSPC) technique was applied for the TR-PL measurements. The light source was a Ti:sapphire laser (MIRA900, Coherent) with 150 fs pulse width, 700 nm wavelength, and the repetition rate of 76 MHz. The beam was frequency doubled to 350 nm by using a β-BaB_2O_4 (BBO) crystal. The PL was dispersed by a 15 cm monochromator and detected by a UV-enhanced multichannel plate photomultiplier tube (MCP-PMT). A commercially available TCSPC module (PicoHarp 300, PicoQuant GmbH) was used to obtain PL decay curves. In general, the full width at half-maximum (fwhm) of total instrument response function (IRF) was less than 130 ps.

Acknowledgment. This research was supported by a grant from the National Research Laboratory program (R0A-2007- 000-20075-0) and Pioneer research program for converging technology (2009-008-1529) and Nano R&D (Grant No. 2009-0082724) through the Korea Science and Engineering Foundation funded by the Ministry of Education, Science & Technology and APRI-Research Program through a grant provided by GIST in 2010 and KIST (2E21552).

Supporting Information Available: Additional TEM images of the Si NSs; structural characterization using XRD measurements; absorbance spectrum and its replotted spectra. This material is available free of charge *via* the Internet at http://pubs.acs.org.

REFERENCES AND NOTES

1. Erogbogbo, F.; Yong, K.-T.; Roy, I.; Xu, G.; Prasad, P. N.; Swihart, M. T. Biocompatible Luminescent Silicon Quantum Dots for Imaging of Cancer Cells. *ACS Nano* **2008,** *2*, 873–878.
2. Zhuang, L.; Guo, L.; Chou, S. Y. Silicon Single-Electron Quantum-Dot Transistor Switch Operating at Room Temperature. *Appl. Phys. Lett.* **1998,** *72*, 1205–1207.
3. Cui, Y.; Lieber, C. M. Functional Nanoscale Electronic Devices Assembled Using Silicon Nanowire Building Blocks. *Science* **2001,** *291*, 851–853.
4. Huang, M. H.; Mao, S.; Feick, H.; Yan, H.; Wu, Y.; Kind, H.; Weber, E.; Russo, R.; Yang, P. Room-Temperature Ultraviolet Nanowire Nanolasers. *Science* **2001,** *292*, 1897–1899.
5. Novoselov, K. S.; Geim, A. K.; Morozov, S. V.; Jiang, D.; Katsnelson, M. I.; Grigorieva, I. V.; Dubonos, S. V.; Firsov, A. A. Two-Dimensional Gas of Massless Dirac Fermions in Graphene. *Nature* **2005,** *438*, 197–200.

6. Zhang, Y.; Tan, Y.-W.; Stormer, H. L.; Kim, P. Experimental Observation of the Quantum Hall Effect and Berry's Phase in Graphene. *Nature* **2005,** *438*, 201–204.
7. Novoselov, K. S.; Jiang, Z.; Zhang, Y.; Morozov, S. V.; Stormer, H. L.; Zeitler, U.; Maan, J. C.; Boebinger, G. S.; Kim, P.; Geim, A. K. Room-Temperature Quantum Hall Effect in Graphene. *Science* **2007,** *315*, 1379.
8. Lu, A. J.; Yang, X. B.; Zhang, R. Q. Electronic and Optical Properties of Single-Layered Silicon Sheets. *Solid State Commun.* **2009,** *149*, 153–155.
9. Morishita, T.; Nishio, K.; Mikami, M. Formation of Single- and Double-Layer Silicon in Slit Pores. *Phys. Rev. B* **2008,** *77*, 081401(R).
10. Okamoto, H.; Kumai, Y.; Sugiyama, Y.; Mitsuoka, T.; Nakanishi, K.; Ohta, T.; Nozaki, H.; Yamaguchi, S.; Shirai, S.; Nakano, H. Silicon Nanosheets and Their Self-Assembled Regular Stacking Structure. *J. Am. Chem. Soc.* **2010,** *132*, 2710–2718.
11. Nakano, H.; Mitsuoka, T.; Harada, M.; Horibuchi, K.; Nozaki, H.; Takahashi, N.; Nonaka, T.; Seno, Y.; Nakamura, Y. Soft Synthesis of Single-Crystal Silicon Monolayer Sheets. *Angew. Chem., Int. Ed.* **2006,** *45*, 6303–6306.
12. Gibson, J. M.; Lanzerotti, M. Y.; Elser, V. Plan-View Transmission Electron Diffraction Measurements of Roughness at Buried Si/SiO_2 Interfaces. *Appl. Phys. Lett.* **1989,** *55*, 1394–1396.
13. Wu, Y.; Cui, Y.; Huynh, L.; Barrelet, C. J.; Bell, D. C.; Lieber, C. M. Controlled Growth and Structures of Molecular-Scale Silicon Nanowires. *Nano Lett.* **2004,** *4*, 433–436.
14. Li, C.-P.; Lee, C.-S.; Ma, X.-L.; Wang, N.; Zhang, R.-Q.; Lee, S.-T. Growth Direction and Cross-Sectional Study of Silicon Nanowires. *Adv. Mater.* **2003,** *15*, 607–609.
15. Kim, B.-S.; Koo, T.-W.; Lee, J.-H.; Kim, D. S.; Jung, Y. C.; Hwang, S. W.; Choi, B. L.; Lee, E. K.; Kim, J. M.; Whang, D. Catalyst-Free Growth of Single-Crystal Silicon and Germanium Nanowires. *Nano Lett.* **2009,** *9*, 864–869.
16. Rivillon, S.; Amy, F.; Chabal, Y. J.; Frank, M. M. Gas Phase Chlorination of Hydrogen-Passivated Silicon Surfaces. *Appl. Phys. Lett.* **2004,** *85*, 2583–2585.
17. Hansen, U.; Vogl, P. Hydrogen Passivation of Silicon Surfaces: A Classical Molecular-Dynamics Study. *Phys. Rev. B* **1998,** *57*, 13295–13304.
18. Markov, I. V. *Crystal Growth for Beginners*; World Scientific: Singapore, 1995; pp 41−62.
19. Wilcoxon, J. P.; Samara, G. A.; Provencio, P. N. Optical and Electronic Properties of Si Nanoclusters Synthesized in Inverse Micelles. *Phys. Rev. B* **1999,** *60*, 2704–2714.
20. Zhang, X.; Neiner, D.; Wang, S.; Louie, A. Y.; Kauzlarich, S. M. A New Solution Route to Hydrogen-Terminated Silicon Nanoparticles: Synthesis, Functionalization and Water Stability. *Nanotechnology* **2007,** *18*, 1–6.
21. Zou, J.; Baldwin, R. K.; Pettigrew, K. A.; Kauzlarich, S. M. Solution Synthesis of Ultrastable Luminescent Siloxane-Coated Silicon Nanoparticles. *Nano Lett.* **2004,** *4*, 1181–1186.
22. Sankaran, R. M.; Holunga, D.; Flagan, R. C.; Giapis, K. P. Synthesis of Blue Luminescnet Si Nanoparticles Using Atmospheric-Pressure Microdischarges. *Nano Lett.* **2005,** *5*, 537–541.
23. Holmes, J. D.; Ziegler, K. J.; Doty, R. C.; Pell, L. E.; Johnston, K. P.; Korgel, B. A. Highly Luminescent Silicon Nanoparticles with Discrete Optical Transitions. *J. Am. Chem. Soc.* **2001,** *123*, 3743–3748.
24. Holmes, J. D.; Johnston, K. P.; Doty, R. C.; Korgel, B. A. Control of Thickness and Orientation of Solution-Grown Silicon Nanowires. *Science* **2000,** *287*, 1471–1473.
25. Choudhury, M. G. M. Optical Properties of Amorphous $Si_{1-x}Ag_x$ Alloys. *J. Phys. C: Solid State Phys.* **1987,** *20*, 2035–2039.
26. Takagahara, T.; Takeda, K. Theory of the Quantum Confinement Effect on Excitons in Quantum Dots of Indirect-Gap Materials. *Phys. Rev. B* **1992,** *46*, 15578–15581.
27. Zhou, Z.; Brus, L.; Friesner, R. Electronic Structure and Luminescence of 1.1- and 1.4-nm Silicon Nanocrystals: Oxide Shell *versus* Hydrogen Passivation. *Nano Lett.* **2003,** *3*, 163–167.
28. Kanemitsu, Y.; Ogawa, T.; Shiraishi, K.; Takeda, K. Visible Photoluminescence from Oxidized Si Nanometer-Sized Spheres: Exciton Confinement on a Spherical Shell. *Phys. Rev. B* **1993,** *48*, 4883–4886.
29. Montazeri, M.; Smith, L. M.; Jackson, H. E.; Yarrison-Rice, J. M.; Choi, Y.-J.; Park, J.-G. Raman Stress Mapping of CdS Nanosheets. *Appl. Phys. Lett.* **2009,** *95*, 083105.
30. Lu, A. J.; Zhang, R. Q.; Lee, S. T. Stress-Induced Band Gap Tuning in ⟨112⟩ Silicon Nanowires. *Appl. Phys. Lett.* **2007,** *91*, 263107.
31. dos Santos, C. L.; Piquini, P. Diameter Dependence of Mechanical, Electronic, and Structural Properties of InAs and InP Nanowires: A First-Principles Study. *Phys. Rev. B* **2010,** *81*, 075408.
32. Banerjee, S.; Datta, A. Photoluminescent Silica Nanotubes and Nanodisks Prepared by the Reverse Micelle Sol−Gel Method. *Langmuir* **2009,** *26*, 1172–1176.
33. Wang, Z.; Quan, Z.; Lin, J. Remarkable Changes in the Optical Properties of CeO_2 Nanocrystals Induced by Lanthanide Ions Doping. *Inorg. Chem.* **2007,** *46*, 5237–5242.